

JointTuner: Appearance-Motion Adaptive Joint Training for Customized Video Generation

Fangda Chen¹, Shanshan Zhao², Chuanfu Xu¹, Long Lan^{1*}

¹College of Computer Science and Technology, National University of Defense Technology

²Alibaba International Digital Commerce

{fdchen.nudt, xuchuanfu, long.lan}@nudt.edu.cn

sshan.zhao00@gmail.com

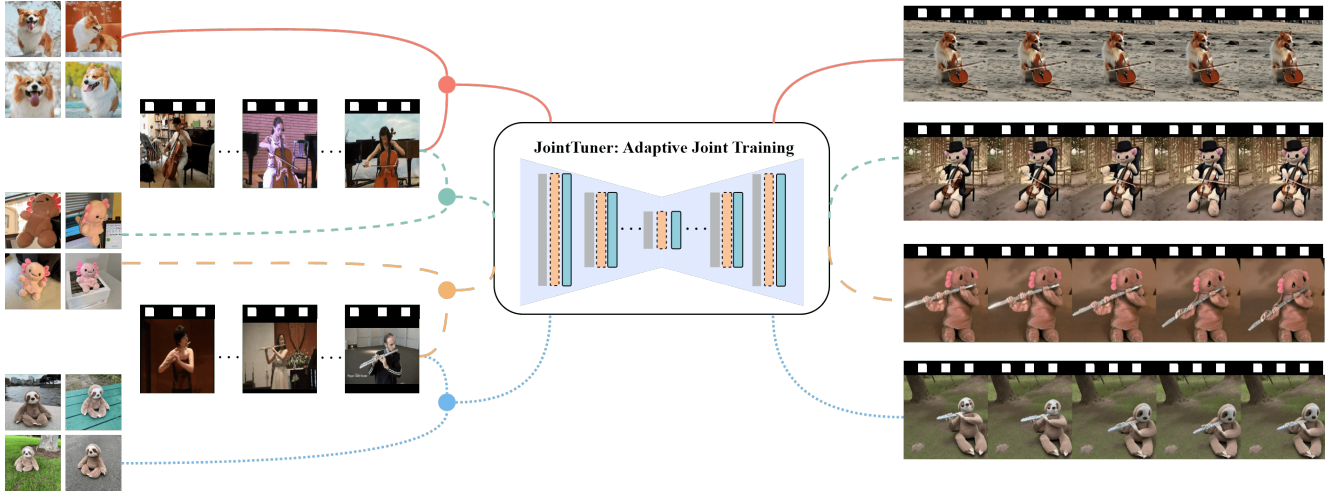


Figure 1. **Customized video generation results of our proposed JointTuner.** With specific appearance-motion paired inputs, JointTuner generate videos with customized subject appearances and motion patterns via adaptive joint training.

Abstract

Recent text-to-video advancements have enabled coherent video synthesis from prompts and expanded to fine-grained control over appearance and motion. However, existing methods either suffer from concept interference due to feature domain mismatch caused by naive decoupled optimizations or exhibit appearance contamination induced by spatial feature leakage resulting from the entanglement of motion and appearance in reference video reconstructions. In this paper, we propose **JointTuner**, a novel adaptive joint training framework, to alleviate these issues. Specifically, we develop **Adaptive LoRA**, which incorporates a context-aware gating mechanism, and integrate the gated LoRA components into the spatial and temporal Transformers within the diffusion model. These components enable simultaneous optimization of appearance and motion, eliminating concept interference. In addition, we introduce the **Appearance-independent Temporal Loss**, which decouples motion patterns from intrinsic appearance in reference video reconstructions through an appearance-

agnostic noise prediction task. The key innovation lies in adding frame-wise offset noise to the ground-truth Gaussian noise, perturbing its distribution, thereby disrupting spatial attributes associated with frames while preserving temporal coherence. Furthermore, we construct a benchmark comprising 90 appearance-motion customized combinations and 10 multi-type automatic metrics across four dimensions, facilitating a more comprehensive evaluation for this customization task. Extensive experiments demonstrate the superior performance of our method compared to current advanced approaches. Project Page: <https://fdchen24.github.io/JointTuner-Website>.

1. Introduction

Recent advancements in text-to-video generation have significantly progressed in synthesizing temporally coherent visual content from textual prompts. Building on these capabilities, the field has expanded its focus to enable fine-grained control. This field has led to the development of appearance customization, which leverage 3-5 reference images to preserve specific appearance characteris-

tics [20, 26, 42, 45], motion customization that extract and transfer motion patterns from reference videos [25, 44, 47], and appearance-motion combined customization that address both aspects [2, 9, 18, 23, 31, 43, 49]. These fields collectively define the emerging paradigm of **Customized Video Generation (CVG)**. Combined customization, as a challenging task that requires simultaneous customization of appearance and motion, becomes the primary focus of this work.

Despite significant progress in appearance-motion customization, existing methods still face limitations in specific scenarios. The prevalent two-stage training paradigm, which separates appearance and motion optimization, often leads to feature domain mismatch during inference, resulting in concept interference in the customized videos. Additionally, motion learning, typically conducted through reference video reconstruction tasks, may inadvertently absorb spatial characteristics due to the entanglement of appearance and motion in the reference videos. These spatial features may cause appearance contamination in customized videos. Further analysis is provided in Sec. 3.1.

To address these limitations, we propose **JointTuner**, an adaptive joint training framework with two key innovations. First, a unified fine-tuning architecture jointly optimizes spatial-temporal features to eliminate feature domain mismatch via the Adaptive LoRA, which incorporates a context-aware gating mechanism for dynamic adaption to different modal inputs (images or videos). Second, we develop the Appearance-independent Temporal Loss (AiT Loss), which decouples motion patterns from intrinsic appearances in reference videos through an appearance-agnostic noise prediction task. By introducing frame-wise offset noise into the ground-truth Gaussian noise, we perturb the ground-truth noise distribution, thereby disrupting spatial attributes associated with frames while preserving temporal coherence.

Furthermore, we introduce a comprehensive evaluation framework for appearance-motion combined customization. Existing datasets focus on appearance customization [19, 32] while the automatic metrics emphasize appearance-alignment quality [2, 43, 49]. For providing a thorough evaluation, we collect 90 appearance-motion customized combinations from publicly available datasets [19, 29, 32, 37, 49]. We also incorporate 10 automatic metrics across four dimensions, including semantic alignment, motion dynamism, temporal consistency, and perceptual quality.

The contributions of this work are as follows:

- We propose JointTuner, a joint training framework that co-optimizes appearance and motion learning using Adaptive LoRA, eliminating the concept interference.
- We introduce Appearance-independent Temporal Loss to mitigate appearance contamination, which decouples motion patterns from intrinsic appearance in the reference

videos via an appearance-agnostic noise prediction task.

- We develop a comprehensive evaluation framework for appearance-motion combined customization, providing reproducible benchmarks and multi-dimensional metrics. Extensive experiments demonstrate the state-of-the-art (SOTA) performance of our method.

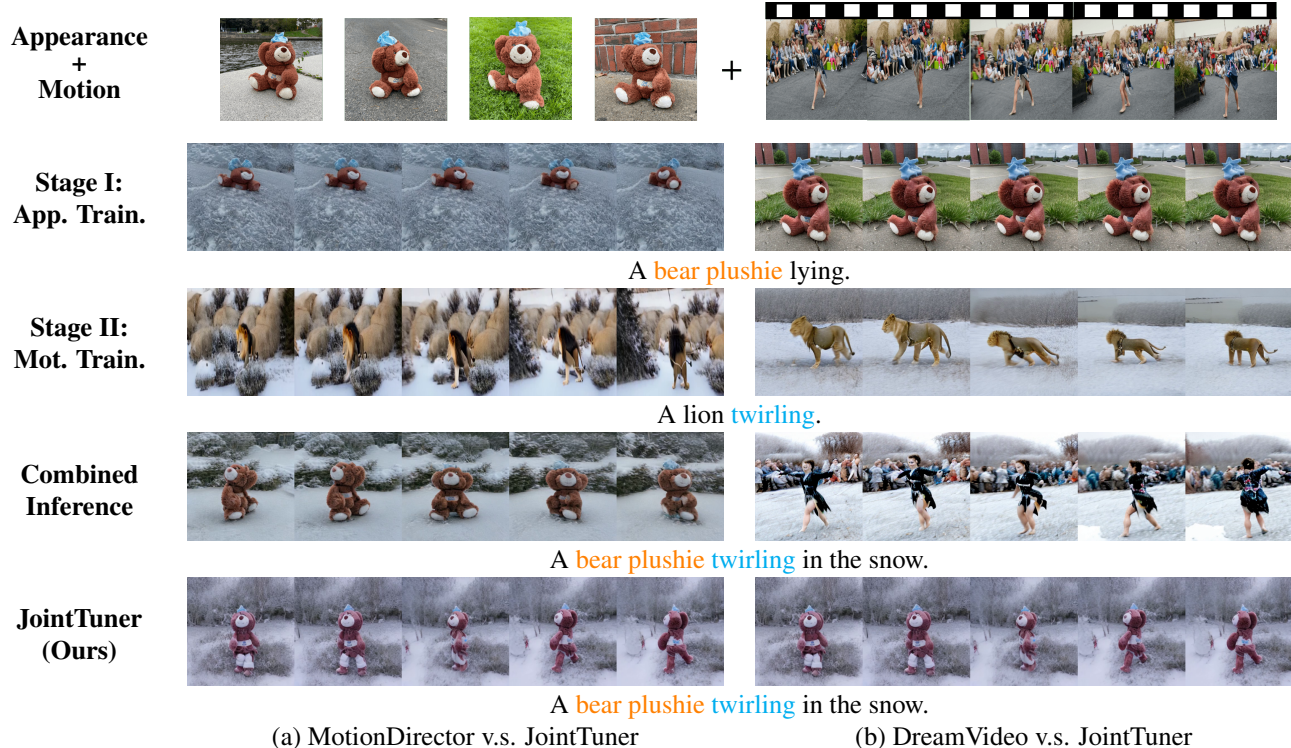
2. Related Work

2.1. Text-to-Video Generation

Early Text-to-Video research primarily employs Generative Adversarial Networks (GANs) [1, 33, 35, 40] and autoregressive models [8, 11, 27]. Recent advancements transition to diffusion-based approaches [4, 16, 34, 48], which currently present advanced performance. AnimateDiff [10] introduces a motion module to animate text-to-image models, enabling high-quality animations. ModelScopeT2V [41] and ZeroScope [38] incorporate spatiotemporal blocks to generate high-fidelity videos. Stable Video Diffusion [3] employs a three-stage training process to further improve video quality. These powerful video generation models offer more possibilities for customized video generation.

2.2. Customized Video Generation

Customized video generation encompasses three primary tasks: appearance customization, motion customization, and appearance-motion combined customization. Appearance customization techniques [20, 26, 42, 45] preserve subject-specific appearance using 3-5 reference images, while motion customization approaches [25, 44, 47] learn motion patterns from reference videos. Appearance-motion combined customization [2, 23, 31, 43, 49] integrate both aspects. For example, MotionDirector [49], MoTrans [23], and Customize-A-Video [31] separately fine-tune spatial and temporal Transformers using LoRA, while DreamVideo[43] employs text inversion and two-stage adapter fine-tuning. However, these methods often suffer from feature domain mismatch during inference, leading to concept interference in customized results. CustomTTT [2] alleviates this issue through layer-specific fine-tuning and test-time tuning. However, it relies on the results of two-stage training and may face the challenge of error accumulation. Additionally, the appearance contamination in motion learning caused by spatial feature leakage remains challenging. Current solutions address this issue in two primary manners. First, parameter replacement mechanisms [31, 49] replace the spatial adaptation modules in motion learning with those in appearance learning during inference. Second, conditioned learning frameworks [43] employ appearance images as auxiliary inputs, enabling the model to learn appearance from conditional signals. However, these methods fail to decouple motion patterns from the appearance of reference videos.



(a) MotionDirector v.s. JointTuner (b) DreamVideo v.s. JointTuner

Figure 2. **The illustration of a failed example from current advanced customized video generation methods.** The first row demonstrates the specified appearance and motion. Subsequent rows showcase the training- and inference-generating videos from MotionDirector[49] and DreamVideo[43]: Appearance Training (**App. Train.**), Motion Training (**Mot. Train.**), and Combined Inference. The bottom row provides the inference results from our JointTuner.

3. Method

This section first introduces relevant preliminaries, including text-to-video diffusion models, low-rank adaptation, and existing appearance-motion combined customization approaches. We then detail JointTuner, focusing on three core components: Adaptive LoRA, One-Frame Spatial Loss, and Appearance-independent Temporal Loss.

3.1. Preliminaries

Text-to-Video Diffusion Model. Following previous customized video generation methods [2, 43, 49], we use a 3D U-Net architecture [6] as the base model. The network (ϵ_θ) includes spatial Transformers for frame-level semantics and temporal Transformers for inter-frame dynamics, jointly optimized with a text encoder (τ_θ) via:

$$\mathbb{E}_{z_0, y, \epsilon, t} [\|\epsilon - \epsilon_\theta(z_t, t, \tau_\theta(y))\|_2^2], \quad (1)$$

where $z_0 \in \mathbf{R}^{F \times H \times W \times C}$ denotes the latent code of the video and F, H, W, C denote the number of frames, height, width, and number of channels of the latent code, y is the text prompt, $\epsilon \sim \mathcal{N}(0, I)$ represents Gaussian noise, and $t \sim \mathcal{U}(0, T)$ corresponds to the diffusion steps.

Low-Rank Adaptation (LoRA). LoRA [12] enables parameter-efficient adaptation by decomposing weight up-

dates as $W = W_0 + BA$, where $W_0 \in \mathbf{R}^{d \times k}$ is frozen, and $B \in \mathbf{R}^{d \times r}$ and $A \in \mathbf{R}^{r \times k}$ (with $r \ll d, k$) are trainable low-rank factors. This modifies forward propagation as follows:

$$x' = W_0 x + \alpha \cdot B A x, \quad (2)$$

reducing trainable parameters while maintaining model capacity. Here, α is a fixed scaling factor.

Appearance-Motion Combined Customization.

Given K reference images and M motion reference videos, the appearance-motion combined customization task aims to synthesize high-fidelity videos that faithfully present the target motion with the specified subject. Current advanced approaches [2, 43, 49] use a two-stage training paradigm, decoupling spatial-temporal feature learning through sequential optimization. In the first stage, appearance-aware tuning parameters in spatial Transformers are optimized using reference images. The spatial alignment loss is defined as:

$$\mathbb{E}_{z_0, y, \epsilon_i, t} [\|\epsilon_i - \epsilon_{\theta, \delta}(z_t, t, \tau_\theta(y))\|_2^2], \quad (3)$$

where ϵ_i denotes the Gaussian noise for image reconstruction and $\epsilon_{\theta, \delta}$ represents the noise predictor with spatial tuning parameters δ and frozen parameters θ . In the second stage, temporal dynamics are captured through motion-

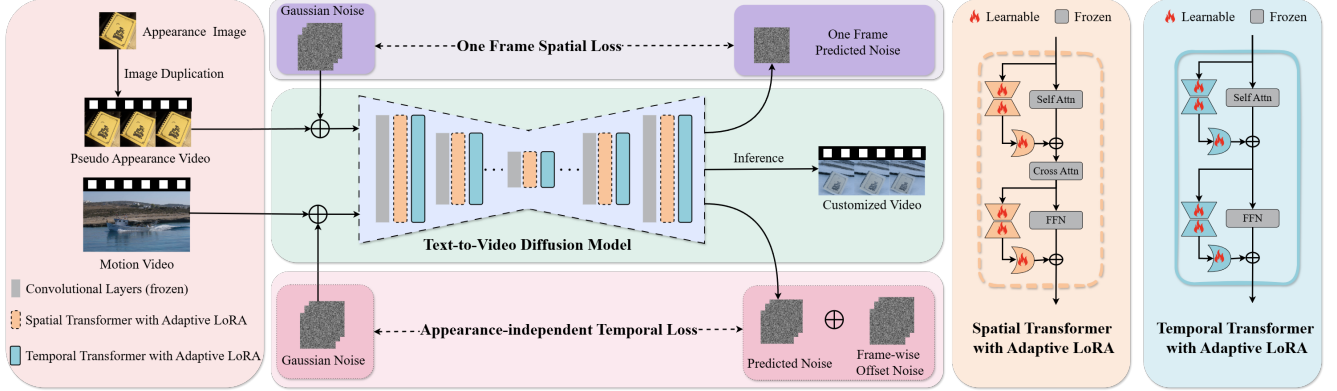


Figure 3. **The architecture of our JointTuner**, an adaptive joint training framework, comprises three parts: (1) **Converting reference images into pseudo-videos** by duplicating frames to match the format of motion videos; (2) **Inserting Adaptive LoRA components** into the spatial and temporal Transformers for parameter-efficient fine-tuning; (3) **Optimizing Adaptive LoRA parameters with two specialized losses**: the One Frame Spatial Loss preserves appearance details, while the Appearance-independent Temporal Loss captures motion patterns. Notably, the pre-trained text-to-video diffusion model remains frozen during training, with only the injected LoRA parameters being fine-tuned. During inference, the trained LoRA weights are loaded to generate customized videos.

aware tuning parameters, optimized via the temporal loss:

$$\mathbb{E}_{z_0, y, \epsilon_v, t} [\|\epsilon_v - \epsilon_{\theta, \kappa}(z_t, t, \tau_\theta(y))\|_2^2], \quad (4)$$

where ϵ_v denotes the Gaussian noise for video reconstruction and $\epsilon_{\theta, \kappa}$ represents the noise predictor with temporal tuning parameters κ and frozen parameters θ . During inference, the denoising process combines both spatial and temporal parameters:

$$z_{t-1} = z_t - \hat{\epsilon}_{\theta, \delta, \kappa}(z_t, t, \tau_\theta(y)), \quad (5)$$

where $\hat{\epsilon}_{\theta, \delta, \kappa}$ denotes the predictor that naively combines δ and κ .

This decoupled paradigm prevents modeling spatiotemporal interactions, as δ and κ train separately on images and videos. The spatial module δ alters feature representations, but the temporal module κ learns motion patterns from original features rather than δ -adapted ones, causing feature domain mismatch. The lack of joint training further leads to spatiotemporal inconsistencies in generated videos, such as mismatched object motion trajectories. As shown in Fig. 2, some approach fails to generate desired customized motions (Fig. 2a) when applied to δ -adapted appearances, as κ never observes adapted spatial features during training. Appearance inconsistencies also emerge in combined scenarios (Fig. 2b), where δ -enhanced visual details degrade due to spatial feature conflicts with the reference spatial features implicitly included in the tuned κ . These failures demonstrate that simple decoupled training is insufficient to resolve the inherent spatiotemporal entanglement, thereby necessitating the joint modeling of appearance and motion.

3.2. Adaptive Joint Training Framework

To address the limitations of concept interference in two-stage adaptation and appearance contamination in motion

learning, we propose JointTuner, which optimizes spatial-temporal features through adaptive joint training. As shown in Fig. 3, we first standardize input representation by temporal extension: images are duplicated to N frames, and videos are uniformly sampled to N frames. Unlike existing methods that sequentially inject spatial and temporal LoRA parameters [49], JointTuner optimizes both simultaneously via Adaptive LoRA, resolving feature domain mismatch through the context-aware gating mechanism. Considering the differences between spatial and temporal features, we use distinct loss functions for different inputs. Specifically, the One-Frame Spatial Loss (OFS Loss) maintains appearance fidelity during appearance learning for images. For videos, the AiT Loss eliminates spatial feature leakage from the reference videos during motion learning. We elaborate on these core designs and provide a detailed analysis in the subsequent subsection.

Adaptive LoRA. As mentioned above, the two-stage training paradigm is confronted with concept interference, and we argue that a joint training framework can resolve this problem. However, using classical LoRA for joint fine-tuning has exhibited certain limitations [2, 43]. One possible reason is that parameter adjustments within the same LoRA may lead to conflicts for two distinct input modalities. To address these issues, we propose Adaptive LoRA equipped with a context-aware gating mechanism, enabling adaptive regulation of LoRA parameters in response to different inputs. This adaptive tuning prevents parameter conflicts within the LoRA and simultaneously optimizes spatial and temporal features. Specifically, the propagation is formulated as follows:

$$x' = W_0 x + \underbrace{\text{Mean}(\sigma(Gx))}_{\text{Dynamic scaling}} \cdot B A x, \quad (6)$$

where G denotes a trainable projection matrix that captures spatial-temporal context, $\sigma(\cdot)$ is the sigmoid activation generating modulation weights, and $Mean(\cdot)$ stabilizes scaling across batches and frames.

One-Frame Spatial Loss. To maintain appearance fidelity during appearance learning, we implement OFS Loss from MotionDirector [49]. By computing reconstruction loss on stochastically isolated frames from duplicated image sequences, the model preserves spatial semantics without overfitting to duplicated frames and is formulated as follows:

$$\mathcal{L}_{\text{OFS}} = \mathbb{E}_{z_0, y, \epsilon_i, t, f} \left[\|\epsilon_i - \epsilon_{\theta, \delta, \kappa}(z_t^f, t, \tau_\theta(y))\|_2^2 \right], \quad (7)$$

where z_t^f denotes the latent code of a randomly sampled frame f from the latent code z_t . Here, we also use δ and κ to denote the Adaptive LoRA parameters in the spatial and temporal Transformers, respectively.

Appearance-independent Temporal Loss. Existing video customization methods face a critical challenge: traditional diffusion loss functions (shown in Eq. (1)) entangle motion and appearance features. This occurs because the 3D U-Net is fine-tuned to minimize reconstruction error based on the whole video latent code, making it difficult to isolate pure motion patterns. To address this fundamental limitation, we propose the AiT Loss that explicitly decouples motion patterns from intrinsic appearance in the reference videos using an appearance-agnostic noise prediction task. As shown in Fig. 3, we first sample standard Gaussian noise $\epsilon_v \sim \mathcal{N}(0, \mathbf{I})$ and add it to the latent code z_t following the diffusion forward process. We then introduce frame-wise offset noise $\epsilon' \sim \mathcal{N}(0, \mathbf{I})$ with dimensions $(1, H, W, 1)$, combined with the ground-truth Gaussian noise ϵ_v to create perturbed targets for noise prediction. The frame-wise perturbations systematically disrupt spatial correlations tied to specific appearances while preserving temporal motion coherence across frames. This forces the model to focus on learning motion patterns independent of the appearance characteristics of reference videos. The AiT loss is defined as follows, and λ is the loss weight:

$$\mathcal{L}_{\text{AiT}} = \lambda \cdot \mathbb{E}_{z_0, y, \epsilon_v, t} \left[\|\epsilon_v + \epsilon' - \epsilon_{\theta, \delta, \kappa}(z_t, t, \tau_\theta(y))\|_2^2 \right]. \quad (8)$$

Analysis. During inference, the system integrates fine-tuned spatial (δ) and temporal (κ) LoRA parameters within the pretrained denoising architecture (implementation details in Supplementary Material Algorithm 1). Our adaptive joint training alternately optimizes δ and κ with corresponding loss functions. This persistent co-adaptation enables temporal modules to learn motion patterns from δ -enhanced features, eliminating the concept interference. As shown in Fig. 2(a), this preserves target motion patterns that two-stage methods fail to reproduce. Additionally, Our AiT Loss eliminates the reference appearance contamination in

the generated videos through an appearance-agnostic noise prediction task, as evidenced in Fig. 2(b).

4. Experiments

In this section, we present our experimental setup, including constructing a benchmark with 90 appearance-motion combinations evaluated through 10 metrics spanning semantic alignment, motion dynamics, temporal consistency, and perceptual quality. We further describe comparative analysis against advanced methods, ablation studies, and hyperparameter sensitivity analysis.

4.1. Settings

Dataset. We construct a more thorough dataset with 90 appearance-motion customization combinations using public datasets [19, 29, 32, 37, 49]. The dataset pairs 15 subjects (classified into rigid, non-humanoid, and humanoid types) with 12 motion types (categorized into rigid, non-human, and human motions with or without props), resulting in six relationship categories. Each combination includes five background renderings to assess generalization, enabling a thorough evaluation of appearance-motion customization performance under diverse conditions. More details are in the Supplementary Material.

Metrics. We establish a comprehensive automatic evaluation framework across four dimensions: (1) *Semantic Alignment*, measured by text-video (**CLIP-T**) and image-video (**CLIP-I**) correspondence, and motion pattern consistency (**Mot-Fid**); (2) *Motion Dynamism*, assessed through motion smoothness (**Mot-Smth**) and intensity (**Dyn-Deg**); (3) *Temporal Consistency*, evaluated via subject (**Subj-Con**) and background (**Bkgd-Con**) stability; and (4) *Perceptual Quality*, quantified by human preference (**Pick-Sc**), aesthetic (**Aesth-Q**), and technical quality (**Img-Q**). Implementation details are provided in the Supplementary Material. Additionally, three composite metrics offer holistic performance assessment:

- **Average Rank Score (ARS):** Mean model ranking score across all ten metrics in the same table.
- **Normalized Average Score (NAS):** Scores normalized against the top-performing baseline (100-point scale) and averaged across metrics.
- **Absolute Average Score (AAS):** Arithmetic mean of raw metric scores.

Implementation Details. The joint training framework uses Adaptive LoRA parameters in diffusion transformers, trained for 2000 iterations with a learning rate of 5×10^{-4} . The AiT Loss weight λ is set to 10 based on hyperparameter analysis. Training requires 17GB GPU memory and takes approximately 30 minutes. Inference uses DDIM [36] with 30 sampling steps to generate 16-frame videos at 8 FPS.

Models (on ZeroScope[38])	Composite Metrics			Semantic Alignment			Motion Dynamism		Temporal Consistency		Perceptual Quality		
	ARS ↓	NAS ↑	AAS ↑	CLIP-T ↑	CLIP-I ↑	Mot-Fid ↑	Mot-Smith ↑	Dyn-Deg ↑	Subj-Con ↑	Bkgd-Con ↑	Pick-Sc ↑	Aesth-Q ↑	Img-Q ↑
MotionDirector [49]	<u>2.00</u>	<u>92.78</u>	<u>62.71</u>	<u>28.56</u>	70.73*	70.12	96.66	34.22	94.12*	94.49*	<u>20.37</u>	<u>53.27</u>	<u>64.62</u>
DreamVideo [43]	2.50	92.27	62.22	27.39	51.70	<u>72.60</u>	<u>96.94</u>	61.56*	89.92	<u>94.10</u>	20.01	48.66	59.33
JointTuner (Ours)	1.50*	96.14*	64.15*	32.14*	<u>62.44</u>	72.61*	97.78*	<u>46.89</u>	<u>91.92</u>	93.83	21.19*	57.14*	65.53*

Table 1. **Quantitative comparison of customized video generation by combining different appearances and motions.** Bold numbers indicate the best performance, while numbers with an underline denote the second-best performance across the evaluated methods.

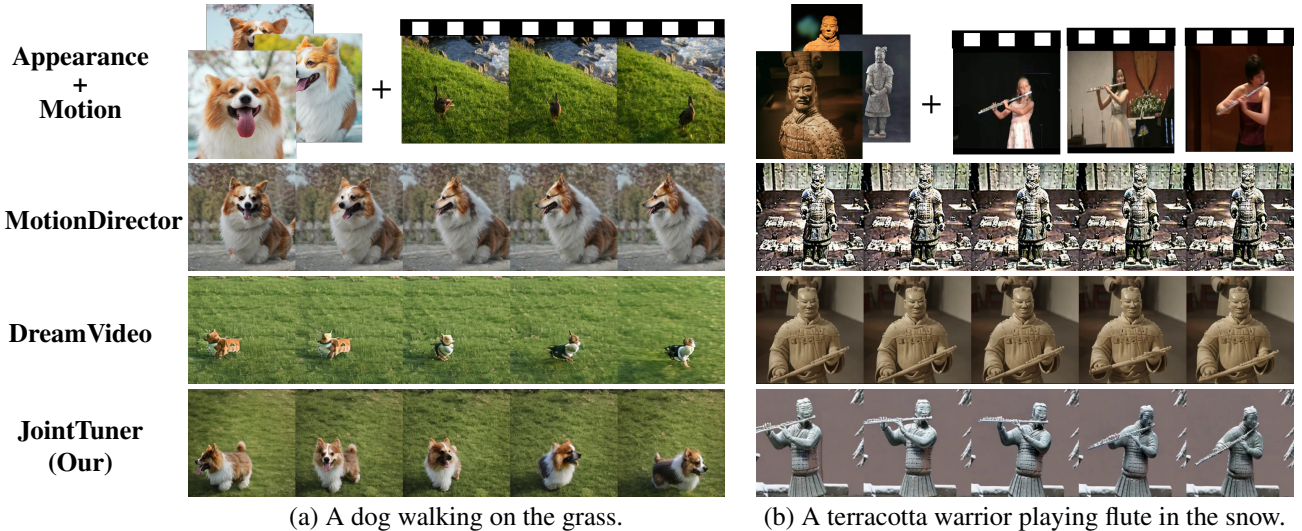


Figure 4. **Qualitative comparison of videos with appearance-motion combined customization.** JointTuner accurately customize both subject appearance and motion patterns, whereas compared methods exhibit partial conceptual interference and appearance contamination.

Customized Video	A dog walking on the grass.				
Models	CLIP-T ↑	CLIP-I ↑	Mot-Fid ↑	Pick-Sc ↑	Subj-Con ↑
MotionDirector [49]	25.49	86.54	68.46	<u>20.03</u>	94.03
DreamVideo [43]	30.22	65.42	94.60	18.95	79.31
JointTuner (Ours)	<u>29.22</u>	<u>76.79</u>	<u>69.61</u>	20.26	<u>87.43</u>

Table 2. **Partial quantitative results for the customized video in the Fig. 4(a).** Bold numbers indicate the best performance, while numbers with an underline denote the second-best performance across the evaluated methods.

4.2. Overall Performance Comparison

Based on the dataset, we compare JointTuner with two open-source models for appearance-motion combined customization: MotionDirector [49] and DreamVideo [43]. Some excellent works require additional control conditions, such as pose sequences. These are not compared here. For a fair comparison, we use the fine-tuned ZeroScope [38] model as the base text-to-video diffusion model for all methods. We also conduct comparative experiments on another pre-trained model, ModelScope[41], with results in the Supplementary Material. The evaluation included both quantitative and qualitative analyses of the experimental results.

Quantitative Analysis. As demonstrated in Tab. 1 and Supplementary Material Tab. A3, our JointTuner both achieve SOTA performance, particularly excelling in per-

ceptual quality. Although our JointTuner does not achieve optimal performance on all metrics, this stems from a significant bias of existing methods towards specific evaluation aspects. To further analyze, we individually evaluate the three customized videos shown in Fig. 4(a). As shown in Tab. 2, we observe that MotionDirector[49] excels in CLIP-I and Subj-Con metrics, indicating superior appearance fidelity and temporal consistency. However, human visual inspection reveals its generated videos exhibit near-static content without desired motion patterns in Fig. 4(a), suggesting CLIP-I and Subj-Con metrics are biased towards static video presentations. Our introduced motion alignment metrics solve this issue, where MotionDirector shows poor performance (low CLIP-T and Mot-Fid scores). Conversely, DreamVideo achieves high Mot-Fid and CLIP-T scores but fails to maintain consistent subject appearance shown in Fig. 4(a), as reflected by its low CLIP-I and Subj-Con values. Our JointTuner demonstrates balanced performance across all metrics, securing the highest Pick-Sc score and ranking second in other metrics. This comprehensive superiority aligns with the qualitative comparisons in Fig. 4(a), confirming our SOTA performance in appearance-motion combined customization. These observations also reveal a critical limitation of conventional appearance-focused metrics for appearance-motion combined customization tasks. Our proposed multi-perspective evaluation metrics provide

Models	Composite Metrics			Semantic Alignment			Motion Dynamism		Temporal Consistency		Perceptual Quality		
	ARS ↓	NAS ↑	AAS ↑	CLIP-T ↑	CLIP-I ↑	Mot-Fid ↑	Mot-Smth ↑	Dyn-Deg ↑	Subj-Con ↑	Bkgd-Con ↑	Pick-Sc ↑	Aesth-Q ↑	Img-Q ↑
Noise-Pixel	4.00	91.51	60.69	31.13	59.80	59.50	98.06*	34.89	<u>92.23</u>	94.17*	20.80	52.82	63.54
Noise-Video	<u>2.70</u>	<u>97.08</u>	<u>64.06</u>	<u>31.19</u>	62.07	<u>75.11</u>	97.54	47.56	91.70	93.54	<u>21.05</u>	<u>56.45</u>	<u>64.43</u>
Noise-Frame (base)	2.30*	97.42*	64.15*	32.14*	<u>62.44</u>	72.61	<u>97.78</u>	46.89	91.92	93.83	21.19*	57.14*	65.53*
-Offset Noise	4.10	96.49	63.86	29.68	60.30	80.08	96.71	49.33	90.82	93.11	20.83	55.04	62.64
-LoRA Gating	5.20	94.22	62.49	28.94	60.18	72.03	96.20	46.89	91.14	93.31	20.46	52.23	63.54
-LoRA Union	4.60	95.16	63.05	28.95	59.89	73.83	96.01	<u>48.89</u>	91.21	93.21	20.35	54.62	63.59
-Joint Training	4.90	92.89	62.26	28.37	69.08*	73.24	95.54	34.67	93.11*	<u>94.01</u>	20.29	51.57	62.68

Table 3. Quantitative ablation studies of each core design in the proposed JointTuner. Bold numbers indicate the best performance, while numbers with an underline denote the second-best performance across the evaluated methods.

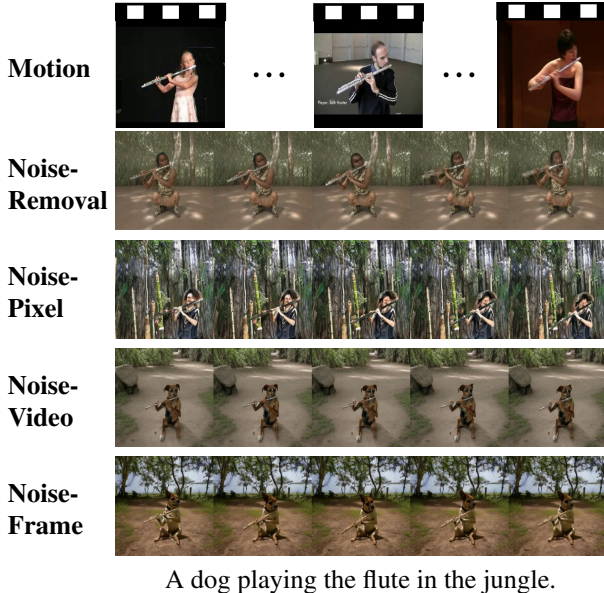


Figure 5. The motion training outcomes using four variants of appearance-agnostic noise prediction task, Noise-Pixel, Noise-Video, Noise-Frame and Noise-Removal.

cost-effective solutions for video generation assessment.

Qualitative Analysis. Visual comparisons in Fig. 4 demonstrate the unique capability of JointTuner for simultaneous appearance-motion customization. MotionDirector [49] generates static outputs with accurate appearances but failed motions, while DreamVideo [43] retains reference appearances despite capturing target motions. In contrast, JointTuner successfully combines specific appearances, such as specific subjects, with complex motions, including human body movements and prop manipulations, producing complete action sequences with temporal coherence. These observations confirm two technical propositions: Adaptive LoRA enables interference-free spatial-temporal feature fusion through parameter adaptation. At the same time, AiT Loss prevents reference appearance contamination via appearance-agnostic noise prediction task. More results are provided in the Supplementary Material.

4.3. Ablation Study

To validate the effectiveness of our core designs, we conduct systematic ablation studies on three critical compo-

nents: **AiT Loss**, **Adaptive LoRA**, and **Joint Learning**. We then progressively remove components from the **Noise-Frame** model: (1) **-Offset Noise**, eliminating frame-wise offset noise in AiT Loss; (2) **-LoRA Gating**, removing both frame-wise offset noise and the LoRA gating mechanism; (3) **-LoRA Union**, replacing the unified LoRA with separate LoRAs for spatial and temporal Transformers.; and (4) **-Joint Training**, ablating all components, including joint training.

AiT Loss Impact. For the **AiT Loss**, we evaluate three noise injection variants: **Noise-Pixel** (pixel-wise offset noise with dimensions $(F, 1, 1, C)$, where C and F denote the number of channels and frames, respectively), **Noise-Video** (video-wise offset noise with dimensions (F, H, W, C)), and **Noise-Frame** (frame-wise offset noise with dimensions $(1, H, W, 1)$). As shown in Tab. 3, the quantitative analysis reveals **Noise-Frame** achieves superior performance across ARS, NAS, and AAS metrics, particularly excelling in semantic alignment and perceptual quality. We investigate the effect of different noise patterns by only the motion customization task, shown in Fig. 5. Our experiments reveal distinct decoupling effects between appearance and motion under different noise conditions. Both **Noise-Video** and **Noise-Frame** demonstrate partial success in disentangling spatial attributes while preserving temporal dynamics, suggesting that frame-level Gaussian noise perturbations effectively suppress appearance information without compromising motion coherence. However, **Noise-Video** and **Noise-Pixel** exhibit degraded background quality in generated sequences, indicating that pixel- and video-level noise perturbations may adversely affect generation quality. We hypothesize that this degradation stems from channel-wise feature corruption, which creates novel latent code distributions that challenge the reconstruction capability of the video decoder during video synthesis. We further compare **Noise-Removal (-Offset Noise)** with the conventional diffusion loss defined in Eq. (1). Experimental results show performance degradation in both CLIP-T and CLIP-I metrics when removing AiT Loss, indicating that AiT Loss enhances appearance customization by reducing the influence of reference video appearance characteristics.

Adaptive LoRA Functionality. We validate Adaptive LoRA effectiveness through quantitative analysis. As

shown in Tab. 3, **-Adaptive LoRA** replacing Adaptive LoRA with basic LoRA present significant performance drops: 26.83% in ARS, 2.35% in NAS, and 2.15% in AAS compared to **-Offset Noise**. These declines across semantic alignment, motion dynamism, and perceptual quality metrics demonstrate Adaptive LoRA impact. To further validate the adaptive importance allocation capability of the Adaptive LoRA components, we conduct quantitative analysis on the gating values across different input modalities (see in Supplementary Material Fig. A1). The adaptive modulation mechanism effectively addresses modality-specific tuning challenges by maintaining an appropriate balance between spatial fidelity and temporal consistency without manual layer selection or weight balancing, demonstrating the capability of Adaptive LoRA to adjust feature importance according to input characteristics automatically.

The Effect of Joint Learning. We analyze joint learning by decomposing it into two components: LoRA union and joint training. As shown in Tab. 3, the variant **-LoRA Union**, fine-tuned using separate classic LoRA (defined in Eq. (2)), outperforms the variant **-LoRA Gating**, which directly applies a unified classic LoRA. However, it underperforms the variant **-Offset Noise**, which leverages Adaptive LoRA-enhanced unified LoRA, across almost all metrics. This indicates that the LoRA union is conditionally effective; the integration of Adaptive LoRA significantly boosts performance by automatically optimizing weight distributions. Additionally, we evaluate a variant without joint training, **-Joint Training**. Compared to **-LoRA Union**, it shows substantial performance degradation: 6.52% in ARS, 2.39% in NAS, and 1.25% in AAS. These results underscore the importance of joint training and its superiority over two-stage training paradigms.

4.4. Hyperparameter study

To evaluate the impact of the AiT Loss weight λ on motion quality in a customized generation, we conduct experiments with varying λ values. We analyze five key metrics related to motion quality, with results visualized in Fig. 6. CLIP-I, Dyn-Deg, and Mot-Fid show significant sensitivity to changes in λ : Dyn-Deg and Mot-Fid improve by 28.68% and 8.86%, respectively, at $\lambda = 10$, while CLIP-I decreases by 13.54%. In contrast, CLIP-T and Pick-Sc exhibit minimal variation, indicating lower sensitivity. Most metrics achieve optimal performance at $\lambda = 10$, with higher Mot-Fid and Dyn-Deg scores reflecting improved motion quality. These results suggest that $\lambda = 10$ is an optimal configuration for this model and can serve as a reference for other customization scenarios.

5. Conclusion and Limitation

In this work, we propose JointTuner, a novel joint training framework addressing two key challenges in customized

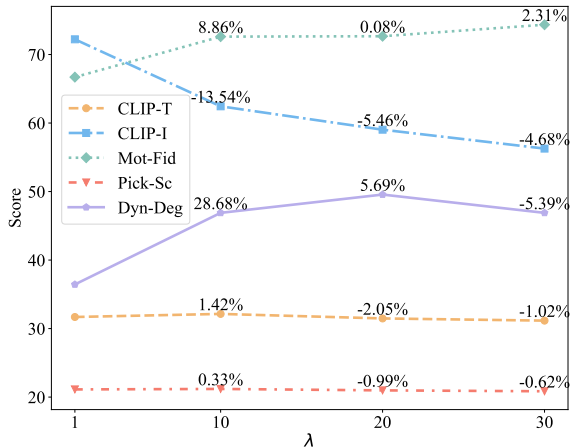


Figure 6. **Quantitative analysis of JointTuner performance with varying AiT loss weight λ .**

video generation: concept interference from feature domain mismatch caused by naive decoupled training and appearance contamination induced by spatial feature leakage due to entanglement of appearance and motion in reference video reconstructions. JointTuner introduces two core innovations: (1) a joint training architecture with Adaptive LoRA, depending on a context-aware gating mechanism, simultaneously optimizing spatial and temporal features and eliminating concept interference, and (2) the Appearance-independent Temporal Loss, which decouples motion patterns from the intrinsic appearances in reference videos through the appearance-agnostic noise prediction task during the video reconstructions. We further establish a comprehensive evaluation framework for appearance-motion combined customization, compressing 90 appearance-motion customization combinations and 10 metrics across four dimensions. Extensive experiments demonstrate the SOTA performance of our JointTuner. Nevertheless, our JointTuner builds upon 3D U-Net architectures. Recent advancements in Diffusion Transformers (DiT) [28] demonstrate superior video generation quality through their inherent scalability and global receptive fields. Adapting our joint training paradigm (particularly the adaptive LoRA gating mechanism) to DiT-based video foundation models while preserving parameter efficiency and motion-appearance disentanglement remains an open challenge. This limitation motivates future exploration of DiT-specific adaptation strategies for combined customization.

References

- [1] Yogesh Balaji, Martin Renqiang Min, Bing Bai, Rama Chellappa, and Hans Peter Graf. Conditional gan with discriminative filter generation for text-to-video synthesis. In *Proceedings of the 28th International Joint Conference on Artificial Intelligence*, pages 1995–2001, 2019. 2
- [2] Xiuli Bi, Jian Lu, Bo Liu, Xiaodong Cun, Yong Zhang, Weisheng Li, and Bin Xiao. Customttt: Motion and appearance customized video generation via test-time training. *arXiv preprint arXiv:2412.15646*, 2024. 2, 3, 4
- [3] Andreas Blattmann, Tim Dockhorn, Sumith Kulal, Daniel Mendelevitch, Maciej Kilian, Dominik Lorenz, Yam Levi, Zion English, Vikram Voleti, Adam Letts, et al. Stable video diffusion: Scaling latent video diffusion models to large datasets. *arXiv preprint arXiv:2311.15127*, 2023. 2
- [4] Andreas Blattmann, Robin Rombach, Huan Ling, Tim Dockhorn, Seung Wook Kim, Sanja Fidler, and Karsten Kreis. Align your latents: High-resolution video synthesis with latent diffusion models. In *Proceedings of the IEEE/CVF Conference on Computer Vision and Pattern Recognition*, pages 22563–22575, 2023. 2
- [5] Mathilde Caron, Hugo Touvron, Ishan Misra, Hervé Jégou, Julien Mairal, Piotr Bojanowski, and Armand Joulin. Emerging properties in self-supervised vision transformers. In *Proceedings of the IEEE/CVF international conference on computer vision*, pages 9650–9660, 2021. 3
- [6] Prafulla Dhariwal and Alexander Nichol. Diffusion models beat gans on image synthesis. *Advances in neural information processing systems*, 34:8780–8794, 2021. 3
- [7] Yuming Fang, Hanwei Zhu, Yan Zeng, Kede Ma, and Zhou Wang. Perceptual quality assessment of smartphone photography. In *Proceedings of the IEEE/CVF conference on computer vision and pattern recognition*, pages 3677–3686, 2020. 3
- [8] Songwei Ge, Thomas Hayes, Harry Yang, Xi Yin, Guan Pang, David Jacobs, Jia-Bin Huang, and Devi Parikh. Long video generation with time-agnostic vqgan and time-sensitive transformer. In *European Conference on Computer Vision*, pages 102–118. Springer, 2022. 2
- [9] Yuchao Gu, Yipin Zhou, Bichen Wu, Licheng Yu, Jia-Wei Liu, Rui Zhao, Jay Zhangjie Wu, David Junhao Zhang, Mike Zheng Shou, and Kevin Tang. Videoswap: Customized video subject swapping with interactive semantic point correspondence. In *Proceedings of the IEEE/CVF Conference on Computer Vision and Pattern Recognition*, pages 7621–7630, 2024. 2
- [10] Yuwei Guo, Ceyuan Yang, Anyi Rao, Zhengyang Liang, Yaohui Wang, Yu Qiao, Maneesh Agrawala, Dahua Lin, and Bo Dai. Animatediff: Animate your personalized text-to-image diffusion models without specific tuning. *International Conference on Learning Representations*, 2024. 2
- [11] Wenyi Hong, Ming Ding, Wendi Zheng, Xinghan Liu, and Jie Tang. Cogvideo: Large-scale pretraining for text-to-video generation via transformers. 2022. 2
- [12] Edward J Hu, Yelong Shen, Phillip Wallis, Zeyuan Allen-Zhu, Yuanzhi Li, Shean Wang, Lu Wang, and Weizhu Chen. Lora: Low-rank adaptation of large language models. 2021. 3
- [13] Ziqi Huang, Yinan He, Jiashuo Yu, Fan Zhang, Chenyang Si, Yuming Jiang, Yuanhan Zhang, Tianxing Wu, Qingyang Jin, Nattapol Chanpaisit, Yaohui Wang, Xinyuan Chen, Limin Wang, Dahua Lin, Yu Qiao, and Ziwei Liu. VBench: Comprehensive benchmark suite for video generative models. In *Proceedings of the IEEE/CVF Conference on Computer Vision and Pattern Recognition*, 2024. 3
- [14] Nikita Karaev, Iurii Makarov, Jianyuan Wang, Natalia Neverova, Andrea Vedaldi, and Christian Rupprecht. CoTracker3: Simpler and better point tracking by pseudo-labelling real videos. In *Proc. arXiv:2410.11831*, 2024. 3
- [15] Junjie Ke, Qifei Wang, Yilin Wang, Peyman Milanfar, and Feng Yang. Musiq: Multi-scale image quality transformer. In *Proceedings of the IEEE/CVF international conference on computer vision*, pages 5148–5157, 2021. 3
- [16] Levon Khachatryan, Andranik Movsisyan, Vahram Tadevosyan, Roberto Henschel, Zhangyang Wang, Shant Navasardyan, and Humphrey Shi. Text2video-zero: Text-to-image diffusion models are zero-shot video generators. In *Proceedings of the IEEE/CVF International Conference on Computer Vision*, pages 15954–15964, 2023. 2
- [17] Yuval Kirstain, Adam Polyak, Uriel Singer, Shahbuland Matiana, Joe Penna, and Omer Levy. Pick-a-pic: An open dataset of user preferences for text-to-image generation. *Advances in Neural Information Processing Systems*, 36:36652–36663, 2023. 3
- [18] Max Ku, Cong Wei, Weiming Ren, Huan Yang, and Wenhu Chen. Anyv2v: A plug-and-play framework for any video-to-video editing tasks. *arXiv preprint arXiv:2403.14468*, 2024. 2
- [19] Nupur Kumari, Bingliang Zhang, Richard Zhang, Eli Shechtman, and Jun-Yan Zhu. Multi-concept customization of text-to-image diffusion. 2023. 2, 5
- [20] Gihyun Kwon and Jong Chul Ye. Tweediemix: Improving multi-concept fusion for diffusion-based image/video generation. *arXiv preprint arXiv:2410.05591*, 2024. 2
- [21] LAION-AI. aesthetic-predictor, 2022. <https://github.com/LAION-AI/aesthetic-predictor>. 3
- [22] Junnan Li, Dongxu Li, Silvio Savarese, and Steven Hoi. Blip-2: Bootstrapping language-image pre-training with frozen image encoders and large language models. In *International conference on machine learning*, pages 19730–19742. PMLR, 2023. 3
- [23] Xiaomin Li, Xu Jia, Qinghe Wang, Haiwen Diao, Mengmeng Ge, Pengxiang Li, You He, and Huchuan Lu. Motrans: Customized motion transfer with text-driven video diffusion models. In *Proceedings of the 32nd ACM International Conference on Multimedia*, pages 3421–3430, 2024. 2
- [24] Zhen Li, Zuo-Liang Zhu, Ling-Hao Han, Qibin Hou, Chun-Le Guo, and Ming-Ming Cheng. Amt: All-pairs multi-field transforms for efficient frame interpolation. In *Proceedings of the IEEE/CVF Conference on Computer Vision and Pattern Recognition*, pages 9801–9810, 2023. 3
- [25] Huijie Liu, Jingyun Wang, Shuai Ma, Jie Hu, Xiaoming Wei, and Guoliang Kang. Separate motion from appearance:

- Customizing motion via customizing text-to-video diffusion models. *arXiv preprint arXiv:2501.16714*, 2025. 2
- [26] Jia-Wei Liu, Yan-Pei Cao, Jay Zhangjie Wu, Weijia Mao, Yuchao Gu, Rui Zhao, Jussi Keppo, Ying Shan, and Mike Zheng Shou. Dynvideo-e: Harnessing dynamic nerf for large-scale motion-and view-change human-centric video editing. In *Proceedings of the IEEE/CVF Conference on Computer Vision and Pattern Recognition*, pages 7664–7674, 2024. 2
- [27] Guillaume Le Moing, Jean Ponce, and Cordelia Schmid. Ccvs: context-aware controllable video synthesis. In *Proceedings of the 35th International Conference on Neural Information Processing Systems*, pages 14042–14055, 2021. 2
- [28] William Peebles and Saining Xie. Scalable diffusion models with transformers. In *Proceedings of the IEEE/CVF international conference on computer vision*, pages 4195–4205, 2023. 8
- [29] F. Perazzi, J. Pont-Tuset, B. McWilliams, L. Van Gool, M. Gross, and A. Sorkine-Hornung. A benchmark dataset and evaluation methodology for video object segmentation. In *Computer Vision and Pattern Recognition*, 2016. 2, 5, 3
- [30] Alec Radford, Jong Wook Kim, Chris Hallacy, Aditya Ramesh, Gabriel Goh, Sandhini Agarwal, Girish Sastry, Amanda Askell, Pamela Mishkin, Jack Clark, et al. Learning transferable visual models from natural language supervision. In *International conference on machine learning*, pages 8748–8763. PMLR, 2021. 3
- [31] Yixuan Ren, Yang Zhou, Jimei Yang, Jing Shi, Difan Liu, Feng Liu, Mingi Kwon, and Abhinav Shrivastava. Customize-a-video: One-shot motion customization of text-to-video diffusion models. In *European Conference on Computer Vision*, pages 332–349. Springer, 2024. 2
- [32] Nataniel Ruiz, Yuanzhen Li, Varun Jampani, Yael Pritch, Michael Rubinstein, and Kfir Aberman. Dreambooth: Fine tuning text-to-image diffusion models for subject-driven generation. In *Proceedings of the IEEE/CVF conference on computer vision and pattern recognition*, pages 22500–22510, 2023. 2, 5
- [33] Xiaoqian Shen, Xiang Li, and Mohamed Elhoseiny. Mostgan-v: Video generation with temporal motion styles. In *Proceedings of the IEEE/CVF Conference on Computer Vision and Pattern Recognition*, pages 5652–5661, 2023. 2
- [34] Uriel Singer, Adam Polyak, Thomas Hayes, Xi Yin, Jie An, Songyang Zhang, Qiyuan Hu, Harry Yang, Oron Ashual, Oran Gafni, et al. Make-a-video: Text-to-video generation without text-video data. 2022. 2
- [35] Ivan Skorokhodov, Sergey Tulyakov, and Mohamed Elhoseiny. Stylegan-v: A continuous video generator with the price, image quality and perks of stylegan2. In *Proceedings of the IEEE/CVF conference on computer vision and pattern recognition*, pages 3626–3636, 2022. 2
- [36] Jiaming Song, Chenlin Meng, and Stefano Ermon. Denoising diffusion implicit models. *arXiv preprint arXiv:2010.02502*, 2020. 5
- [37] K Soomro. Ucf101: A dataset of 101 human actions classes from videos in the wild. *arXiv preprint arXiv:1212.0402*, 2012. 2, 5, 3
- [38] Spencer Sterling. Zeroscope, 2023. https://huggingface.co/cerspense/zeroscope_v2_576w. 2, 6
- [39] Zachary Teed and Jia Deng. Raft: Recurrent all-pairs field transforms for optical flow. In *Computer Vision–ECCV 2020: 16th European Conference, Glasgow, UK, August 23–28, 2020, Proceedings, Part II 16*, pages 402–419. Springer, 2020. 3
- [40] Sergey Tulyakov, Ming-Yu Liu, Xiaodong Yang, and Jan Kautz. Mocogan: Decomposing motion and content for video generation. In *Proceedings of the IEEE conference on computer vision and pattern recognition*, pages 1526–1535, 2018. 2
- [41] Jiuniu Wang, Hangjie Yuan, Dayou Chen, Yingya Zhang, Xiang Wang, and Shiwei Zhang. Modelscope text-to-video technical report. *arXiv preprint arXiv:2308.06571*, 2023. 2, 6, 3, 4
- [42] Zhao Wang, Aoxue Li, Lingting Zhu, Yong Guo, Qi Dou, and Zhenguo Li. Customvideo: Customizing text-to-video generation with multiple subjects. *arXiv preprint arXiv:2401.09962*, 2024. 2
- [43] Yujie Wei, Shiwei Zhang, Zhiwu Qing, Hangjie Yuan, Zhiheng Liu, Yu Liu, Yingya Zhang, Jingren Zhou, and Hongming Shan. Dreamvideo: Composing your dream videos with customized subject and motion. In *Proceedings of the IEEE/CVF Conference on Computer Vision and Pattern Recognition*, pages 6537–6549, 2024. 2, 3, 4, 6, 7
- [44] Jay Zhangjie Wu, Yixiao Ge, Xintao Wang, Stan Weixian Lei, Yuchao Gu, Yufei Shi, Wynne Hsu, Ying Shan, Xiaohu Qie, and Mike Zheng Shou. Tune-a-video: One-shot tuning of image diffusion models for text-to-video generation. In *2023 IEEE/CVF International Conference on Computer Vision (ICCV)*, pages 7589–7599. IEEE Computer Society, 2023. 2
- [45] Tao Wu, Yong Zhang, Xintao Wang, Xianpan Zhou, Guangcong Zheng, Zhongang Qi, Ying Shan, and Xi Li. Customcrafter: Customized video generation with preserving motion and concept composition abilities. *arXiv preprint arXiv:2408.13239*, 2024. 2
- [46] Danah Yatim, Rafail Fridman, Omer Bar-Tal, Yoni Kasten, and Tali Dekel. Space-time diffusion features for zero-shot text-driven motion transfer. In *Proceedings of the IEEE/CVF Conference on Computer Vision and Pattern Recognition*, pages 8466–8476, 2024. 3
- [47] Hidir Yesiltepe, Tuna Han Salih Meral, Connor Dunlop, and Pinar Yanardag. Motionshop: Zero-shot motion transfer in video diffusion models with mixture of score guidance. *arXiv preprint arXiv:2412.05355*, 2024. 2
- [48] Yabo Zhang, Yuxiang Wei, Dongsheng Jiang, Xiaopeng Zhang, Wangmeng Zuo, and Qi Tian. Controlvideo: Training-free controllable text-to-video generation. *arXiv preprint arXiv:2305.13077*, 2023. 2
- [49] Rui Zhao, Yuchao Gu, Jay Zhangjie Wu, David Junhao Zhang, Jia-Wei Liu, Weijia Wu, Jussi Keppo, and Mike Zheng Shou. Motiondirector: Motion customization of text-to-video diffusion models. In *European Conference on Computer Vision*, pages 273–290. Springer, 2024. 2, 3, 4, 5, 6, 7

JointTuner: Appearance-Motion Adaptive Joint Training for Customized Video Generation

Supplementary Material

A. Algorithmic Details

In this section, we show the details of JointTuner and two-stage training paradigm in Algorithm 1 and Algorithm 2.

Algorithm 1: JointTuner

Input : Training data (images and videos), pretrained model weights
Output: Trained model, generated video

- 1 Initialize models: *vae*, *text_encoder*, *unet*;
- 2 Load pretrained model weights;
- 3 Add Adaptive LoRA parameters to *unet*;
- 4 **Training**: Adaptive joint training;
- 5 **for each epoch do**
- 6 **for each batch in data loader do**
- 7 **if batch is image then**
- 8 Duplicate image into video;
- 9 Convert batch to latent space z_t ;
- 10 Sample noise ϵ_i and add to z_t ;
- 11 Encode text embeddings $\tau_\theta(y)$;
- 12 **if batch is image then**
- 13 Compute OFS loss with predicted noise:

$$\mathbb{E}_{z_0, y, \epsilon_i, t, f} [\|\epsilon_i - \epsilon_{\theta, \delta, \kappa}(z_t^f, t, \tau_\theta(y))\|_2^2]$$
- 14 **else if batch is video then**
- 15 Compute AiT loss with predicted noise:

$$\lambda \cdot \mathbb{E}_{z_0, y, \epsilon_v, t} [\|(\epsilon_v + \epsilon') - \epsilon_{\theta, \delta, \kappa}(z_t, t, \tau_\theta(y))\|_2^2]$$
- 16 Update Adaptive LoRA parameters δ and κ ;
- 17 Save trained Adaptive LoRA checkpoints;
- 18 **Inference**: Generating customized videos;
- 19 **for each prompt do**
- 20 Initialize pipeline with pretrained models;
- 21 Load trained adaptive LoRA parameters δ , κ ;
- 22 Prepare input latents (random noise);
- 23 For the latents z_t :
- 24
$$\epsilon_{\theta, \delta, \kappa}(z_t, t, \tau_\theta(y)) = \text{unet}(z_t, t, \tau_\theta(y); \theta, \delta, \kappa)$$
- 25 Denoise the latents using the predicted noise:

$$z_{t-1} = z_t - \epsilon_{\theta, \delta, \kappa}(z_t, t, \tau_\theta(y))$$
- 26 Generate video from the denoised latents;

Algorithm 2: Two-stage Training Method

Input : Training data (images and videos), pretrained model weights
Output: Trained model, generated video

- 1 Initialize models: *vae*, *text_encoder*, *unet*;
- 2 Load pretrained model weights;
- 3 Add tuning parameters to *unet*;
- 4 **Stage I**: Appearance training with images;
- 5 **for each epoch do**
- 6 **for each batch in data loader do**
- 7 Convert batch to latent space z_t ;
- 8 Sample noise ϵ_i and add to z_t ;
- 9 Encode text embeddings $\tau_\theta(y)$;
- 10 Compute spatial loss with predicted noise:

$$\mathbb{E}_{z_0, y, \epsilon_i, t} [\|\epsilon_i - \epsilon_{\theta, \delta}(z_t, t, \tau_\theta(y))\|_2^2]$$
- 11 Update spatial tuning parameters δ ;
- 12 Save trained spatial tuning checkpoints;
- 13 **Stage II**: Motion training with videos;
- 14 **for each epoch do**
- 15 **for each batch in data loader do**
- 16 Convert batch to latent space z_t ;
- 17 Sample noise ϵ_v and add to z_t ;
- 18 Encode text embeddings $\tau_\theta(y)$;
- 19 Compute temporal loss with predicted noise:

$$\mathbb{E}_{z_0, y, \epsilon_v, t} [\|\epsilon_v - \epsilon_{\theta, \kappa}(z_t, t, \tau_\theta(y))\|_2^2]$$
- 20 Update temporal tuning parameters κ ;
- 21 Save trained temporal tuning checkpoints;
- 22 **Combined Inference**: Generating videos;
- 23 **for each prompt do**
- 24 Initialize pipeline with pretrained models;
- 25 Load trained spatial tuning parameters δ ;
- 26 Load trained temporal tuning parameters κ ;
- 27 Prepare input latents (random noise);
- 28 For the latents z_t :
- 29
$$\epsilon_{\theta, \delta, \kappa}(z_t, t, \tau_\theta(y)) = \text{unet}(z_t, t, \tau_\theta(y); \theta, \delta, \kappa)$$
- 30 Denoise the latents using the predicted noise:

$$z_{t-1} = z_t - \epsilon_{\theta, \delta, \kappa}(z_t, t, \tau_\theta(y))$$
- 31 Generate video from the denoised latents;

Category	Description	Samples
Rigid Subject	No limbs, non-deformable	guitar (CustomDiffusion/instrument_music2), book (CustomDiffusion/things_book), car (CustomDiffusion/transport_car6), backpack (DreamBooth/backpack_dog), clock (DreamBooth/clock)
Non-Humanoid Subject	No standing limbs	cat (CustomDiffusion/pet_cat5), wolf_plushie (DreamBooth/wolf_plushie), tortoise_plushie (CustomDiffusion/plushie_tortoise), unicorn_toy (CustomDiffusion/toy_unicorn), dog (DreamBooth/dog)
Humanoid Subject	Standing limbs with articulation	pink_plushie (CustomDiffusion/plushie_pink), bear_plushie (DreamBooth/bear_plushie), sloth_plushie (DreamBooth/grey_sloth_plushie), monster_toy (DreamBooth/monster_toy), terracotta_warrior (MotionDirector/Terracotta_Warrior)
Rigid Motion	Object-level movement	boat_sailing (DAVIS2016/boat), bus_traveling (DAVIS2016/bus), train_turning (DAVIS2016/train)
Non-Human Motion	Animal-like locomotion	bear_walking (DAVIS2016/bear), duck_walking (DAVIS2016/mallard-fly), dog_walking (DAVIS2016/dog)
Human Motion (Without Props)	Body-only actions	person_dancing (DAVIS2016/breakdance-flare), person_twirling (DAVIS2016/dance-twirl), person_walking (DAVIS2016/kite-walk)
Human Motion (With Props)	Multi-video sequences (5 clips per motion)	person_lifting_barbell (UCF101/CleanAndJerk), person_playing_cello (UCF101/PlayingCello), person_playing_flute (UCF101/PlayingFlute)

Table A1. **Categorization and sample source of subjects and motions in the dataset.**

Subject Category	Compatible Motion Categories
Rigid Subject	Rigid Motion
Non-Humanoid Subject	Non-Human Motion Human Motion (Without Props) Human Motion (With Props)
Humanoid Subject	Human Motion (Without Props) Human Motion (With Props)

Table A2. **Valid pairing relationships between subject categories and motion categories in the dataset.**

The fundamental differences between our joint training framework (Algorithm 1) and the two-stage training method (Algorithm 2) are systematically analyzed through four key aspects:

- **Training Strategy:** JointTuner (Algorithm 1) employs joint training where image and video data are processed in a unified loop with adaptive parameter sharing. In contrast, Two-stage training method (Algorithm 2) adopts sequential training, separating appearance learning (Stage I) and motion learning (Stage II).
- **Parameter Adaptation:** JointTuner simultaneously updates spatial-temporal parameters (δ, κ) through **Adaptive LoRA**, while Two-stage training method independently optimizes spatial (δ) and temporal (κ) parameters

in separate stages, risking suboptimal coordination.

- **Loss Design:** JointTuner introduces **AiT Loss** with frame-wise offset noise (ϵ') and **OFS Loss** for joint optimization, whereas Two-stage training method uses decoupled spatial and temporal losses without explicit motion-appearance interaction.
- **Inference:** JointTuner achieves single-pass generation using unified parameters, while Two-stage training method requires dual-parameter fusion ($\delta + \kappa$), potentially introducing concept interference.

B. Dataset Constructions

This section describes the structure and preprocessing of our collected dataset.

B.1. Dataset Composition

As detailed in Tab. A1, the dataset integrates 15 subjects from CustomDiffusion [19], DreamBooth [32], and MotionDirector [49], along with 9 motions from DAVIS2016 [29] and 3 composite motions with multiple video instances (each containing 5 clips) from UCF101 [37]. We construct 6 distinct pairing configurations between subjects and motions, as shown in Tab. A2. Additionally, we set 5 distinct background settings for evaluation, including natural envi-

ronments (grassland, jungle, snowscape) and urban settings (beachfront, cobblestone streets). This results in 90 combinations of subject and motion samples, which, combined with the 5 background settings, produce 450 customized videos.

B.2. Data Preprocessing

Each motion video is preprocessed to standardize its format. For the DAVIS2016 [29] dataset, keyframes are extracted every 2 frames, resulting in videos with a frame rate of 8 FPS, 16 frames, and a duration of 2 seconds. For the UCF101 [37] dataset, keyframes are extracted every 6 frames, yielding videos with the same frame rate (8 FPS), frame count (16 frames), and duration (2 seconds). The original video resolution is retained. Subsequently, each video is annotated using BLIP-2 ¹ [22] to generate descriptive captions.

C. Experiment Settings

C.1. Comparison Methods

This subsection details the implementation of the models used for comparison.

- **MotionDirector** [49]: We use the settings from the official implementation of MotionDirector ². For appearance learning, the spatial LoRA is trained for 1,000 iterations at a learning rate of 5.0×10^{-4} . For motion learning, the temporal LoRA is trained for 3,000 iterations at 5.0×10^{-4} for multi-reference motions and 300 iterations for single-reference motions. During inference, 16-frame videos at 8 FPS are generated using DDIM with 30 sampling steps.
- **DreamVideo** [43]: We follow the settings from the official implementation of DreamVideo ³. For appearance learning, the text identity is optimized for 3,000 iterations at 1.0×10^{-4} , and the identity adapter is trained for 1,000 iterations at 1.0×10^{-5} . For motion learning, the motion adapter is trained for 1,000 iterations at 1.0×10^{-5} for multi-reference motions and 3,000 iterations for single-reference motions. During inference, 16-frame videos at 8 FPS are generated using DDIM with 50 sampling steps and classifier-free guidance.

C.2. Evaluating Metrics

We establish a comprehensive evaluation framework across four dimensions: semantic alignment, motion dynamism, temporal consistency, and perceptual quality, using ten metrics. Three composite indicators provide holistic performance assessment.

¹<https://github.com/salesforce/LAVIS/tree/main/projects/blip2>

²<https://github.com/showlab/MotionDirector>

³<https://github.com/ali-vilab/VGen>

Semantic Alignment

- **CLIP-Text (CLIP-T)**: Measures text-video alignment via frame-wise cosine similarity between CLIP [30] embeddings of input prompts and generated frames.
- **CLIP-Image (CLIP-I)**: Evaluates visual-semantic correspondence using CLIP [30] image encoder to compare reference images and generated frames.
- **Motion-Fidelity (Mot-Fid)**: Assesses motion pattern consistency using CoTracker3 [14] via diffusion-motion-transfer [46].

Motion Dynamism

- **Motion-Smoothness (Mot-Smth)**: Evaluates temporal coherence using video interpolation priors from AMT [24] via VBench [13].
- **Dynamic-Degree (Dyn-Deg)**: Quantifies motion intensity using optical flow estimation via RAFT [39] within VBench [13].

Temporal Consistency

- **Subject-Consistency (Subj-Con)**: Tracks object persistence using DINO [5] feature similarity via VBench [13].
- **Background-Consistency (Bkgd-Con)**: Evaluates background stability using CLIP [30] feature similarity across frames.

Perceptual Quality

- **Pick-Score (Pick-Sc)**: Predicts human preference scores using PickScore [17] with frame-level averaging.
- **Aesthetic-Quality (Aesth-Q)**: Measures artistic merit using LAION aesthetic predictor [21] via VBench [13].
- **Imaging-Quality (Img-Q)**: Evaluates technical quality using MUSIQ [15] trained on SPAQ [7].

D. More Results

In this section, we first present the quantitative comparison of our JointTuner based on the ModelScope[41] foundation model with current advanced methods. As shown in Tab. A3, our JointTuner still achieves the best performance. We then demonstrate our exploration of the specific effects of Adaptive LoRA. Finally, we provide additional qualitative analyses to compare the performance differences between our JointTuner and current advanced methods.

In this part, we conduct quantitative analysis on gating values across different input modalities, to further validate the adaptive importance allocation capability of the Adaptive LoRA component. Using 30 appearance-motion combinations with multi-clip videos, we track the gating responses in spatial and temporal Transformer layers during joint training (see Fig. A1). Fig. A1(a-b) present heatmaps of gating values under image and video inputs respectively, where warmer colors indicate greater gating values and higher importance weights. Two critical observations emerge: (1) Spatial Transformer layers consistently exhibit larger gating values than temporal counterparts across both input types, suggesting that spatial fea-

Models (on ModelScope[41])	Composite Metrics			Semantic Alignment			Motion Dynamism		Temporal Consistency		Perceptual Quality		
	ARS ↓	NAS ↑	AAS ↑	CLIP-T ↑	CLIP-I ↑	Mot-Fid ↑	Mot-Smth ↑	Dyn-Deg ↑	Subj-Con ↑	Bkgd-Con ↑	Pick-Sc ↑	Aesth-Q ↑	Img-Q ↑
MotionDirector	<u>2.20</u>	92.98	61.81	<u>28.91</u>	68.00*	67.42	96.01	37.56	92.40*	93.41	<u>20.34</u>	<u>51.04</u>	<u>63.05</u>
DreamVideo	2.30	<u>93.76</u>	<u>62.31</u>	27.69	54.44	78.44*	<u>96.16</u>	51.11*	91.22	94.85	20.10	48.69	60.41
JointTuner	1.50*	97.42*	63.88*	32.08	<u>63.31</u>	<u>69.65</u>	97.50*	<u>48.44</u>	<u>91.47</u>	<u>93.43</u>	21.10*	56.50*	65.33*

Table A3. **Quantitative comparison of customized video generation by combining different appearances and motions.** Bold numbers indicate the best performance, while numbers with an underline denote the second-best performance across the evaluated methods.

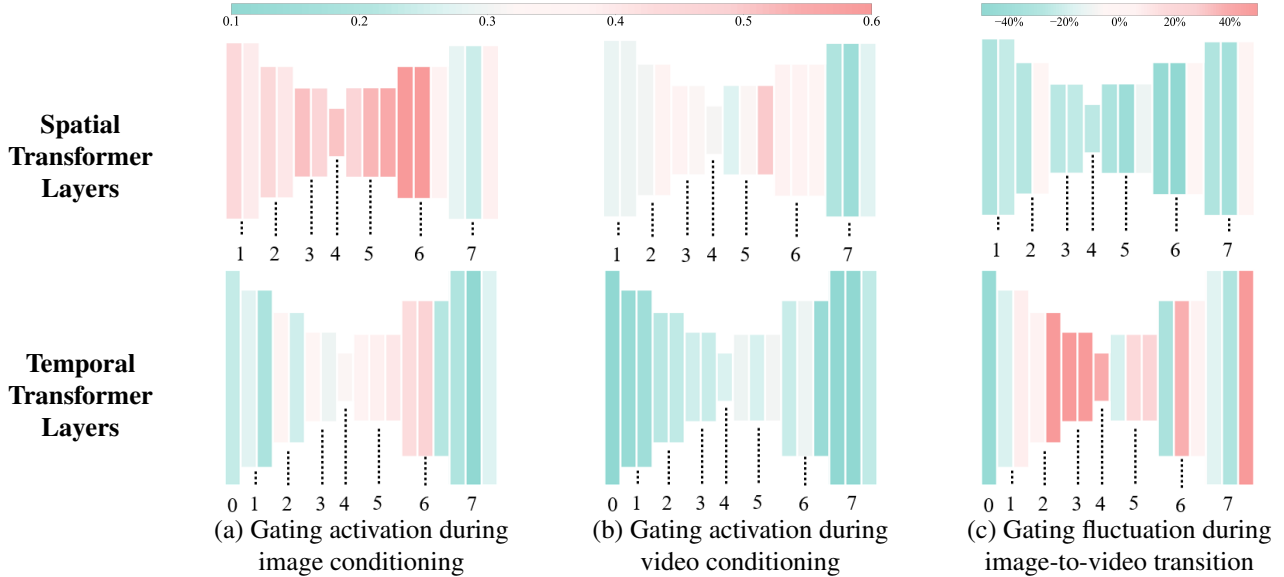


Figure A1. **Visualization of the gating values of Adaptive LoRA across 3D U-Net layers.** (a) and (b) display heatmaps for image and video inputs respectively, where warmer colors indicate higher gating values (stronger activation) and cooler colors denote lower values. (c) presents a difference map for image-to-video input transition comparisons, with warm colors marking increased gating values and cool colors indicating decreased values.

ture adaptation requires more meticulous fine-tuning regardless of input modality. This implies the necessity to decouple spatial characteristics in video inputs to prevent appearance interference with motion learning; (2) The 5th and 6th Transformer layers in the 3D U-Net demonstrate predominant importance in LoRA adaptation, which aligns with the layer-specific sensitivity patterns observed in [2]. Fig. A1(c) analyzes importance redistribution when switching from image to video inputs, where warmer colors denote increased importance and cooler colors represent decreased weights. Temporal Transformer layers exhibit prominent warm-toned regions while spatial layers show cooler tones. This visual evidence confirms Adaptive LoRA dynamically shifts its focus: prioritizing spatial feature preservation for image inputs while emphasizing temporal coherence adaptation for video inputs. The adaptive modulation mechanism effectively addresses modality-specific tuning challenges by maintaining appropriate balance between spatial fidelity and temporal consistency without manual layer selection or weight balancing, demonstrating Adaptive LoRA’s capability to automatically adjust feature importance according to input characteristics.

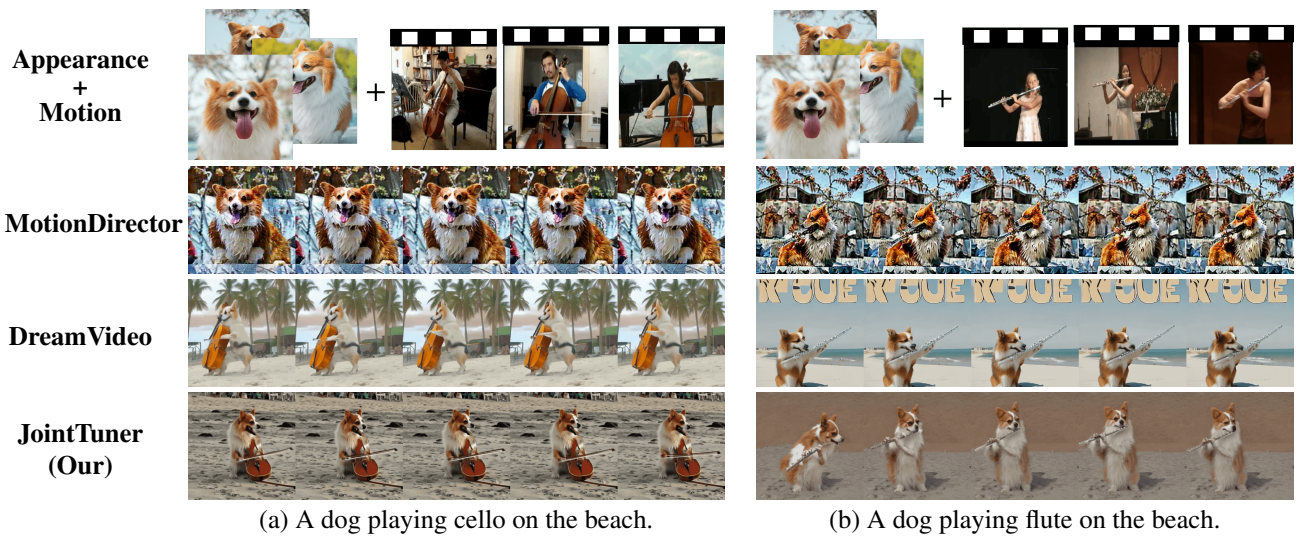


Figure A2. Qualitative comparison of videos with appearance-motion combined customization.

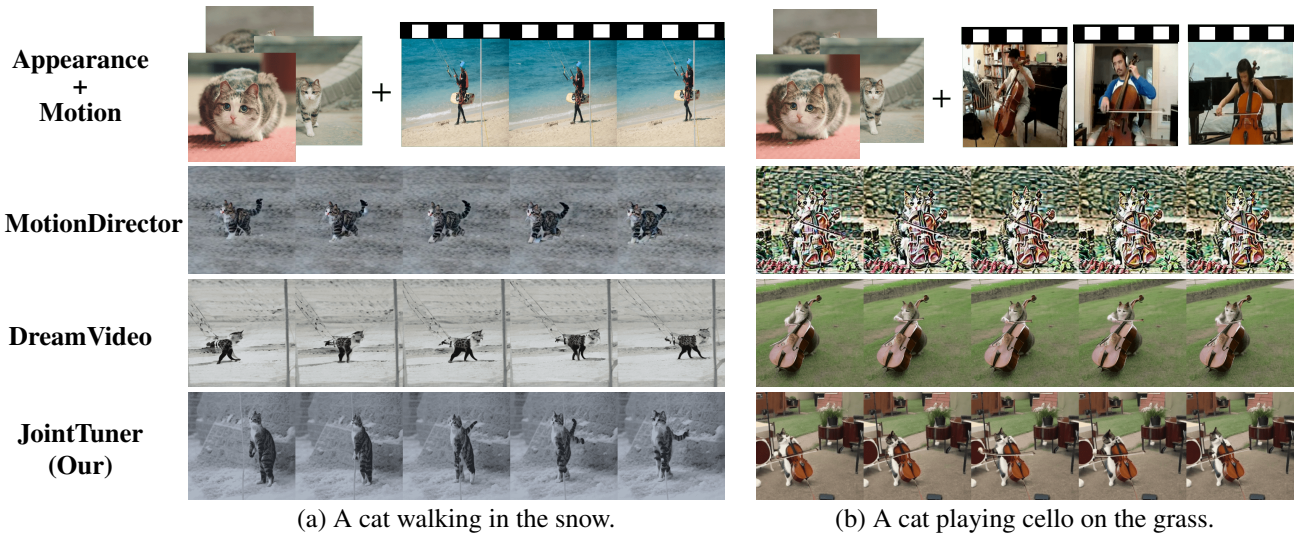
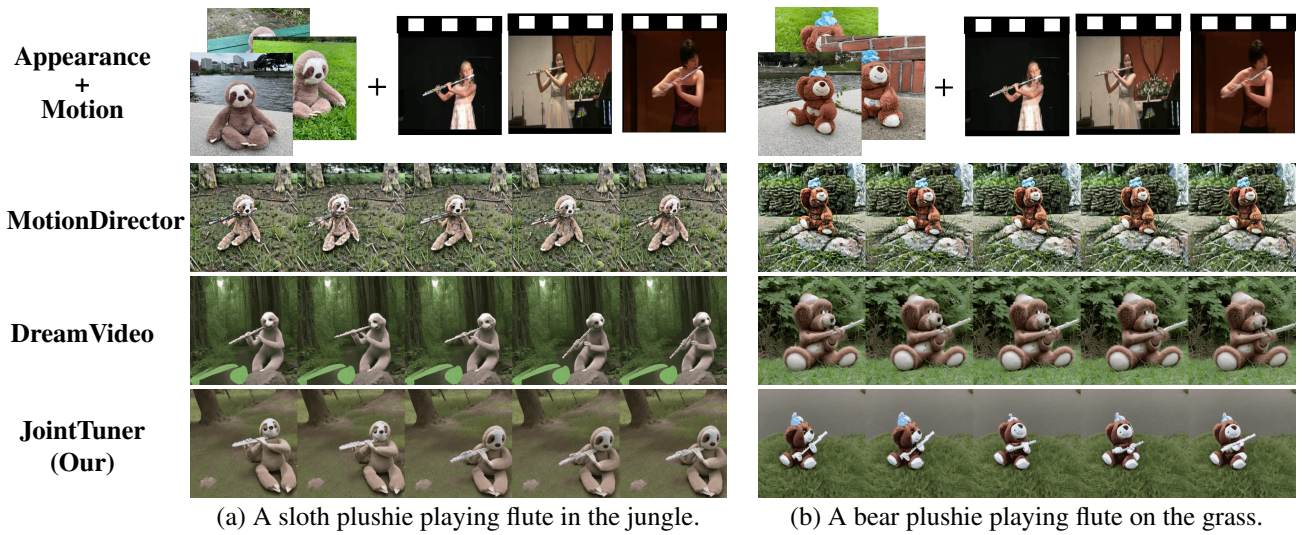


Figure A3. Qualitative comparison of videos with appearance-motion combined customization.



(a) A sloth plushie playing flute in the jungle.

(b) A bear plushie playing flute on the grass.

Figure A4. Qualitative comparison of videos with appearance-motion combined customization.